Dynamics of charged particles in bifurcated current sheets : the k=1 regime.

Dominique C. Delcourt, H.V. Malova, L.M. Zelenyi

Dynamics of charged particles in bifurcated current sheets: The $\kappa \approx 1$ regime

D. C. Delcourt
CETP-CNRS-IPSL, Saint-Maur des Fossés, France

H. V. Malova and L. M. Zelenyi
Space Research Institute, Russian Academy of Sciences, Moscow, Russia

Received 29 July 2003; revised 26 September 2003; accepted 18 November 2003; published 30 January 2004.

[1] We examine the nonlinear dynamics of charged particles in the double-hump current sheets that develop during the late growth phase of substorms. We focus on particles for which the adiabaticity parameter κ (defined as the square root of the minimum curvature radius to maximum Larmor radius ratio) is of the order of unity. We show that as in the case of a simple parabolic field reversal, the magnetic moment scattering experienced by these particles may be described as the result of perturbation of the gyromotion by an impulsive centrifugal force. Here however the double-hump structure of the current sheet leads to two successive centrifugal perturbations, which has a significant impact on the net change of magnetic moment. In a single-hump current sheet, three distinct regimes of magnetic moment variations are obtained for a given value of κ, namely, systematic enhancement at small pitch angles, negligible change at large pitch angles, and in between either damping or enhancement depending upon gyration phase. In contrast, in a double-hump current sheet, repeated application of this three-branch pattern can lead to magnetic moment damping for particles that previously experience magnetic moment enhancement and vice versa. The gyrophase gain both during and between the centrifugal impulses is found to play an essential role in the net magnetic moment change. In particular, in contrast to single-hump current sheets, the $\kappa \approx 1$ limit may be characterized by quasi-adiabatic behavior with negligible variations of the magnetic moment. *INDEX TERMS:* 7807 Space Plasma Physics: Charged particle motion and acceleration; 7843 Space Plasma Physics: Numerical simulation studies; 2744 Magnetospheric Physics: Magnetotail; 2788 Magnetospheric Physics: Storms and substorms; 2772 Magnetospheric Physics: Plasma waves and instabilities; *KEYWORDS:* double hump current sheets, single particle dynamics, centrifugal impulse model, numerical simulations

Citation: Delcourt, D. C., H. V. Malova, and L. M. Zelenyi (2004), Dynamics of charged particles in bifurcated current sheets: The $\kappa \approx 1$ regime, *J. Geophys. Res.*, *109*, A01222, doi:10.1029/2003JA010167.

1. Introduction

[2] Numerous studies indicate that thin current sheets (TCS) are common phenomena in the Earth's magnetosphere [e.g., *Mitchell et al.*, 1990; *Pulkkinen et al.*, 1994; *Sergeev et al.*, 1998]. Such TCS are observed both near the plasma sheet inner edge [e.g., *Runov et al.*, 2003a] and in the distant magnetotail in the vicinity of the neutral line [e.g., *Hoshino et al.*, 1996]. Properties of these TCS include a characteristic thickness that varies from a few hundreds of km up to a few thousands of kilometers [e.g., *Sergeev et al.*, 1993a; *Nakamura et al.*, 2002; *Runov et al.*, 2003b] as well as metastability [*Galeev and Zelenyi*, 1975]. Recent observations in the midtail [e.g., *Asano et al.*, 2003; *Runov et al.*, 2003b; *Sergeev et al.*, 2003] reveal that in some instances, these TCS have a "bifurcated" or "double-hump" structure. Such a structure is at variance with that of "single-hump" current sheets which are commonly postulated in the geomagnetic tail [e.g., *Harris*, 1962]. The physical mechanism at the origin of such a bifurcation in the current sheet structure remains unclear. As an example, *Hoshino et al.* [1996] suggested that this structure may result from "demagnetized" ion dynamics near the distant *X*-line combined with significant Hall electron current on both sides of the midplane. *Zelenyi et al.* [2002] proposed another mechanism for current sheet bifurcation whereby the current carried by ions executing Speiser-type orbits [*Speiser*, 1965] is gradually altered by that of nonadiabatic quasi-trapped ions. This ultimately leads to current reduction at the sheet center, an effect which was viewed as a natural "aging" process. *Greco et al.* [2002] also suggested that current bifurcation may result from chaotic particle scattering due to magnetic fluctuations.

[3] Because the geometry of double-hump current sheets radically differs from that of single-hump ones, we anticipate significant deviations in the nonadiabatic behavior of charged particles. In this paper, we restrict ourselves to

0148-0227/04/2003JA010167

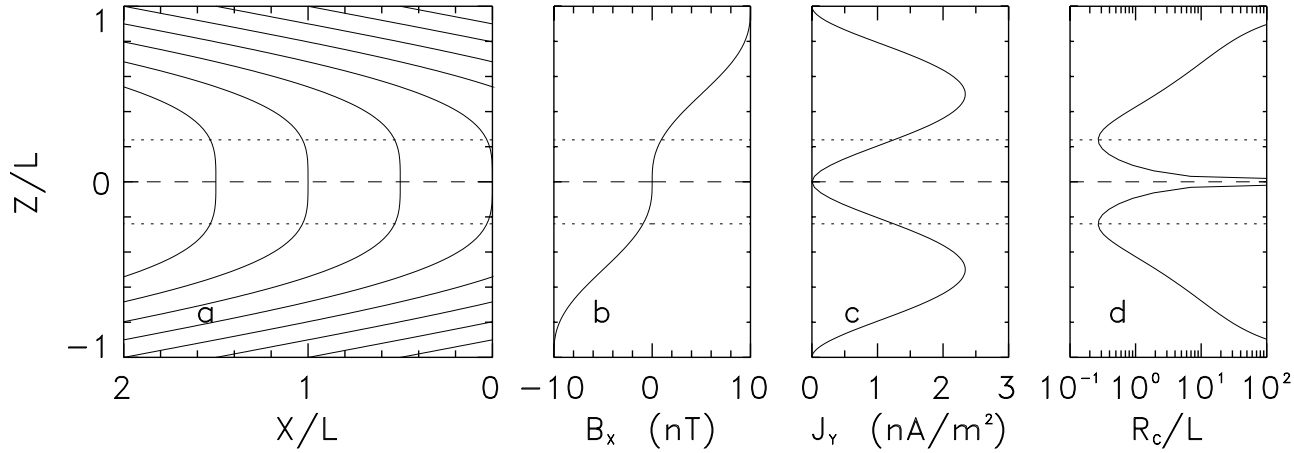

Figure 1. (from left to right) Magnetic field lines in a model double-hump current sheet (equation (1)), B_X component, current density, and field line curvature radius (normalized to the half-thickness of the current sheet) versus Z height. In each panel, dotted lines show the Z height of the maximum field line curvature.

cases where the adiabaticity parameter κ is of the order of unity (equivalently, to relatively weak field reversals or to particles with relatively low energy). We thus exclude from consideration particles that experience fast oscillations about the midplane. We will demonstrate that the net magnetic moment change experienced by the particles can be viewed as the result of successive elemental scattering sequences and that each of these sequences can be described using the centrifugal impulse interpretation framework developed for the single-hump case. We will also show that gyro-phase effects play an essential role, leading to a wide variety of particle behaviors. In section 2, we will discuss results of single particle trajectory computations, whereas the centrifugal impulse based interpretation will be presented in section 3.

2. Magnetic Moment Scattering in a Model Double-Hump Current Sheet

[4] In order to examine the behavior of charged particles in a double-hump configuration, we adopt the following simple description for the magnetic field:

$$B_X = B_o\left[10\frac{Z^3}{L^3} - 15\frac{Z^4}{L^4} + 6\frac{Z^5}{L^5}\right] \tag{1a}$$

$$B_Z = B_n. \tag{1b}$$

Here L is the current sheet half-thickness, B_n, the small component of the magnetic field normal to the midplane, and B_o, the asymptotic B_X component in the lobe. Note that the polynomial description in equation (1a) is such that $dB_X/dZ = 0$ at both $Z = 0$ and $Z = L$, which ensures smooth B_X variations throughout the field reversal. The field line geometry achieved from equation (1) can be appreciated in Figure 1 where B_o, B_n and L are set to 10 nT, 2 nT and 1 R_E, respectively. The double-hump nature of the current sheet in equation (1a) is clearly apparent from Figure 1c which shows the current density as a function of Z height. Two current maxima are noticeable at $Z = \pm 0.5\ L$, or equivalently at $B_X = \pm 0.5\ B_o$ (Figure 1b). This current density variation leads to a specific geometry of the magnetic field lines with a curvature that maximizes at some distance on either side of the midplane (Figure 1d). As implicit in the magnetic field line equation $dX = [B_X/B_Z]\ dZ$, the locus of this curvature maximum depends upon both L and B_o/B_n ratio. It occurs at a Z height of $\sim$0.24 L with the above model parameters (horizontal dotted line in Figure 1). The geometry portrayed in Figure 1 contrasts with that of a single-hump field reversal (e.g., the parabolic one with $B_X = B_oZ/L$) where the magnetic field line curvature is maximum at the equator. In other words, in contrast to the single-hump case where both B and R_C reach a minimum at $Z = 0$, the weak field region in the double-hump case does not coincide with that of maximum curvature. As will be seen hereinafter, this is of importance when describing non-adiabatic episodes during transport.

[5] A parameter that is widely used to characterize the behavior of charged particles in a single-hump field reversal is the parameter κ introduced by *Büchner and Zelenyi* [1989], which is defined as the square root of the minimum curvature radius-to-maximum Larmor radius ratio. For given field model parameters and particle energy, this parameter κ determines all possible behaviors of the particles. For instance, for κ between 1 and 3, the variations of the particle magnetic moment, μ, are organized according to a three-branch pattern (see, e.g., Figure 1 of *Delcourt et al.* [1996a]), namely, at small pitch angles, particles experience systematic μ enhancement regardless of their initial phase of gyration (oblique branch). At large pitch angles, particles experience negligible μ change (horizontal branch) whereas, at intermediate pitch angles, either μ enhancement or damping is obtained depending upon gyration phase (vertical branch). For a given value of κ, these three distinct branches are prescribed and particles evolve from one branch to another during their successive crossings of the field reversal (see Figure 3 of *Delcourt et al.* [1996b]). Moreover, as κ decreases from 3 toward unity, this three-branch pattern gradually expands into the velocity space,

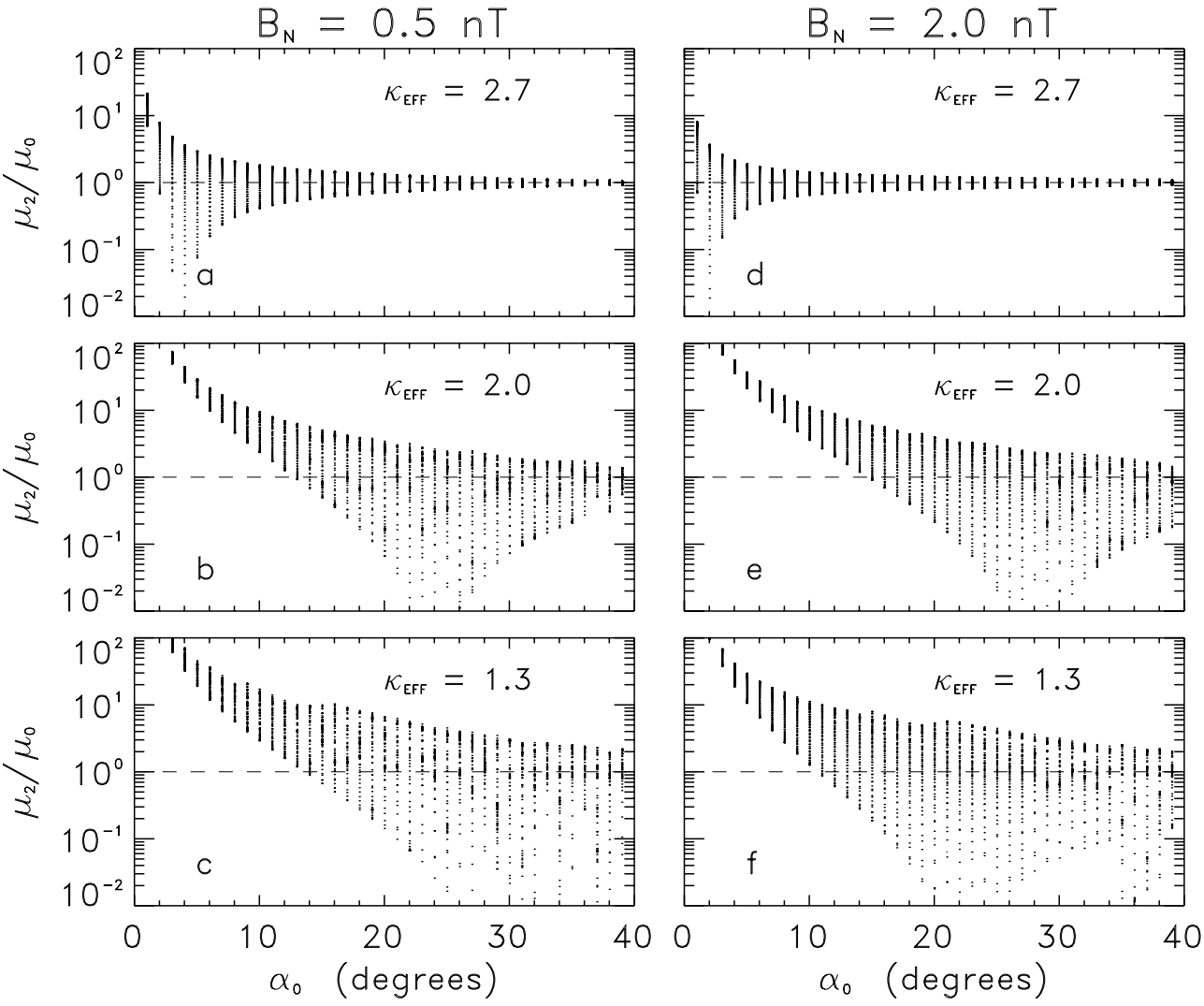

Figure 2. Final magnetic moment as a function of initial pitch angle (at Z_K and in the adiabatic limit) for three distinct values of κ_{eff}: (from top to bottom) 2.7, 2.0, and 1.3. Left and right panels correspond to two different values of B_n (namely, 0.5 and 2.0 nT, respectively).

the vertical branch with μ damping occurring at larger and larger pitch angles (see Figure 1 of *Delcourt et al.* [1996a]).

[6] For $\kappa > 3$, particles are transported adiabatically and the guiding center approximation is valid. This nearly coincides with the adiabatic limit reported by *Sergeev et al.* [1993b], which reads $k = \kappa^2 \approx 8$. On the other hand, for $\kappa < 1$, particles may experience meandering motion about the field minimum as initially shown by *Speiser* [1965]. Even though these meandering trajectory sequences are not adiabatic stricto senso, they do have some regularity with the action integral $I_Z = \int \dot{Z} dZ$ as a local invariant during the $Z = 0$ crossing. *Büchner and Zelenyi* [1989] interpreted the overall particle behavior as the result of successive jumps of this action integral upon separatrix crossing. Using Poincaré surfaces of section, *Chen and Palmadesso* [1986] pointed out that at $\kappa < 1$, the phase space is partitioned into distinct regions, namely, transient (Speiser-type), stochastic (quasi-trapped) and trapped orbits, each of them being characterized by different time scales. This phase space partition is obtained regardless of the field reversal geometry [e.g., *Chen et al.*, 1990a] and directly depends upon the value of κ (or, equivalently, of the dimensionless Hamiltonian). For specific values of κ, *Chen and Palmadesso* [1986] pointed out that the regions of transient (Speiser-type) orbits are more developed. This behavior results from resonance between the fast Z-oscillations about the midplane and the slow gyromotion due to the small B_Z [e.g., *Burkhart and Chen*, 1991] and it is responsible for modulations in observed velocity distributions [e.g., *Chen et al.*, 1990b; *Holland et al.*, 1999].

[7] In a single-hump field reversal such as the parabolic one or the Harris sheet, the above κ parameter is calculated at $Z = 0$ which is the locus of both minimum curvature radius and maximum Larmor radius ρ_L. In contrast, in a double-hump field geometry, the minimum curvature radius does not occur at $Z = 0$ but somewhat off-equator (see Figure 1). At this latter position, the B magnitude is larger than its equatorial value and one thus cannot minimize both R_C and B to compute κ. We suspect however that the particle dynamics will depend upon the maximum curvature of the field reversal and, for reasons that will become more obvious

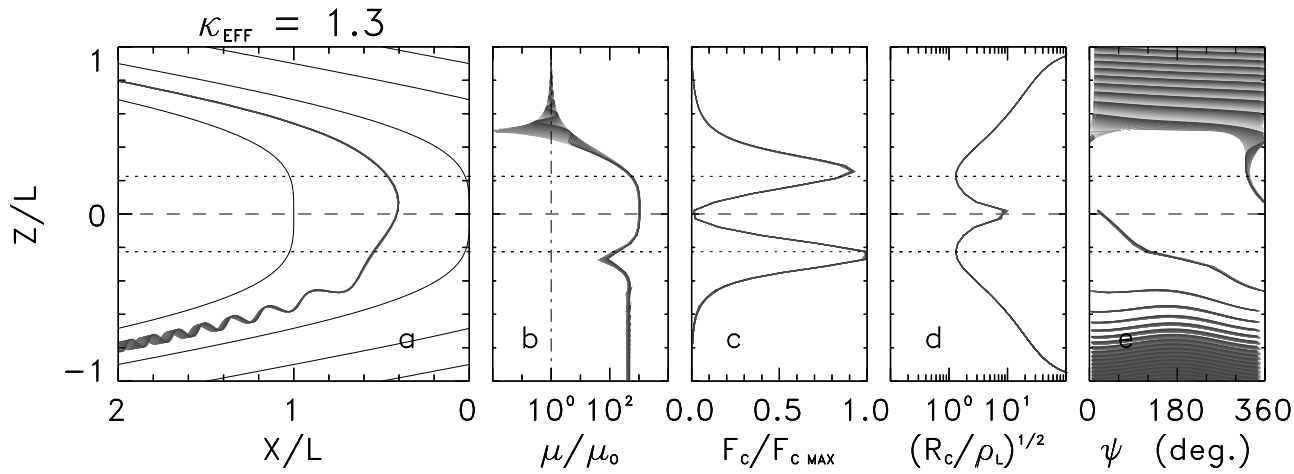

Figure 3. Model particle orbits in the double-hump geometry given by equation (1): (from left to right) trajectory projection in the *X-Z* plane, magnetic moment (normalized to the initial value), centrifugal force (normalized to the maximum value), curvature radius-to-Larmor radius ratio, and gyration phase versus *Z* height. The particles are launched with 2° pitch angle (at Z_K and in the adiabatic limit). The various grey levels correspond to different initial phases of gyration (from 0° to 360° by steps of 10°). The κ_{eff} parameter is set to 1.3.

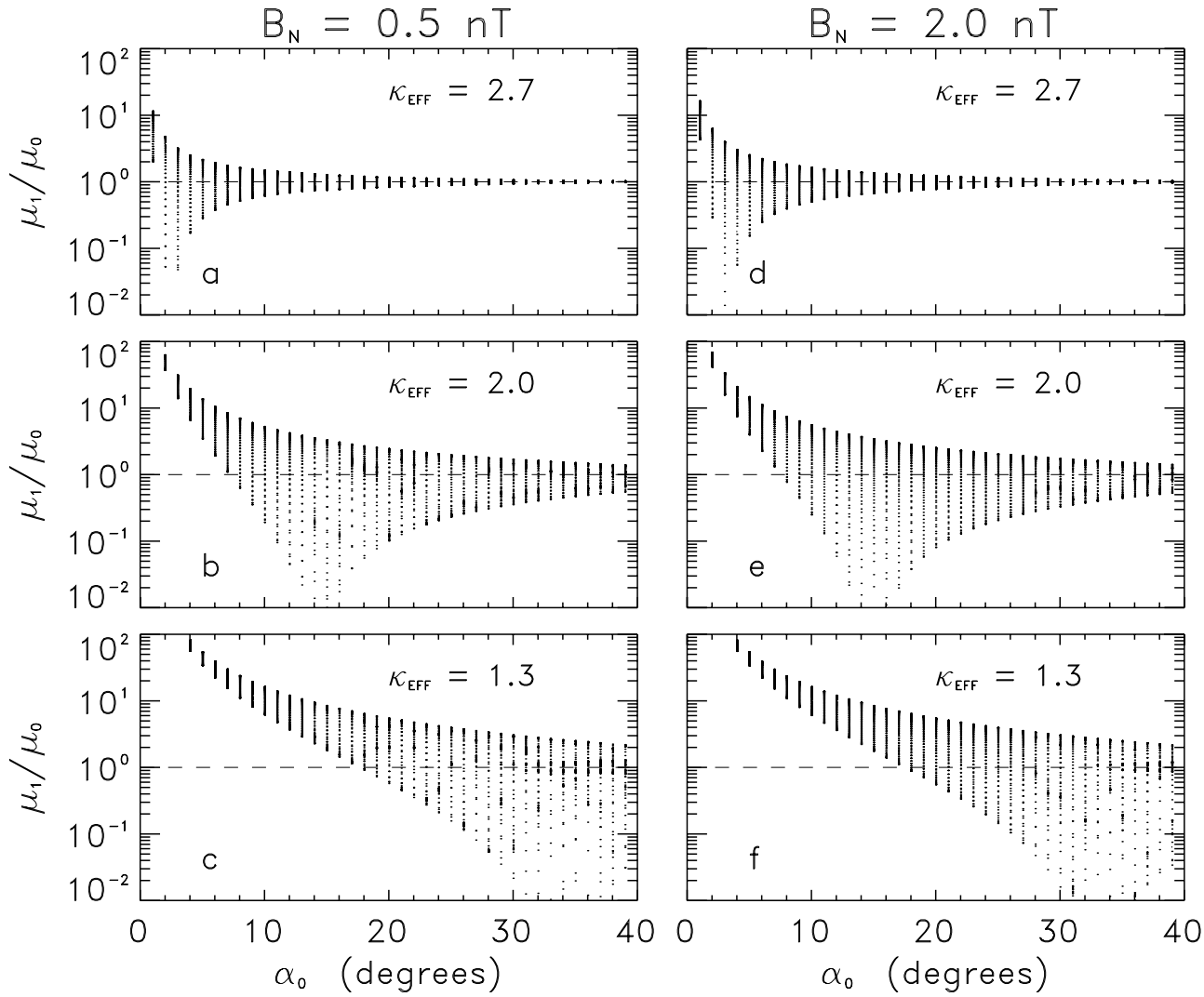

Figure 4. Identical to Figure 2 but for the magnetic moment at $Z = 0$, i.e., immediately after crossing of the first hump.

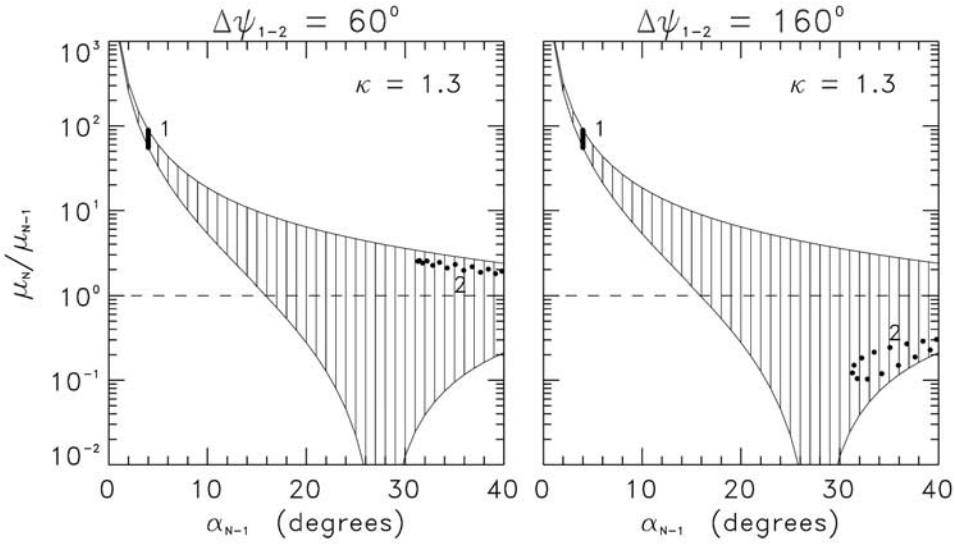

Figure 5. Analytical magnetic moment variations after two successive centrifugal impulses, assuming an initial pitch angle of 4°. The various dots correspond to different initial phases of gyration (from 0° to 360° by steps of 20°). Left and right panels relate to different phase changes between the two impulses (namely, 60° and 160°, respectively). The hatched area in each panel shows the envelope of magnetic moment changes obtained within the centrifugal impulse model. The κ_{eff} parameter is set to 1.3.

in section 3, we introduce an effective parameter κ_{eff} which is the minimum value of the $[R_C/\rho_L]^{1/2}$ ratio encountered along the field line (note that in this ratio, the whole velocity of the particle is assumed to be in the perpendicular direction). This κ_{eff} parameter is thus identical to κ but is evaluated at a Z height (denoted by Z_K hereinafter) different than $Z = 0$. Note here that, for given model parameters B_o, B_n and L, the minimum curvature radius R_C is smaller in a single-hump reversal than in a double-hump one. As an example, with the above parameter values, one has $R_C = 0.2\ L$ in the parabolic field and $R_C \sim 0.27\ L$ in Figure 1. Accordingly, for given particle energy, κ is somewhat larger in a double-hump geometry than in a single-hump one.

[8] The results of numerical trajectory calculations in the above double-hump configuration (Figure 1) are shown in Figure 2. Here, test ions were launched from various positions above the equator, considering different initial phases of gyration ψ (from 0° up to 360° by steps of 5°) and pitch angles α. The centrifugal impulse interpretation framework (see section 3) leads us to consider Z_K as a Z height of reference when defining these initial pitch angles, their value at a different Z height being computed from μ conservation in first approximation. In Figure 2, initial pitch angles are such that their values at Z_K using μ conservation vary from 0° up to 40° (by steps of 1°). The trajectories throughout the field reversal were calculated using the full equation of motion. They were interrupted at mirror point ($\alpha = 90°$) or when the particles reach the opposite edge of the current sheet ($Z = -L$). Three different values of κ_{eff} were considered in Figure 2, namely, 2.7 (equivalently, near the adiabatic-nonadiabatic transition), 2.0 and 1.3. Also, two different magnitudes of B_n were used (left and right panels of Figure 2), which yields two different particle energies for given κ_{eff} value. Figure 2 shows the final magnetic moment (normalized to the initial value) of the particles as a function of initial pitch angle. For clarity, this magnetic moment after crossing of the two humps will be denoted as μ_2 in the following, whereas μ_1 will denote the magnetic moment at $Z = 0$ (equivalently, after crossing of the first hump) and μ_0, the initial one. Similarly, α_0 will denote the initial pitch angle, α_1, the pitch angle after crossing of the first hump, and α_2, the final pitch angle, all of them being evaluated at the reference height Z_K using μ conservation.

[9] The examination of Figure 2 reveals significant deviations from the single-hump case. As an example, in the right panels ($B_n = 2$ nT), a clear three-branch pattern can be seen for $\kappa_{eff} = 2$ (Figure 2e), which contrasts with the more complex pattern obtained for $\kappa_{eff} = 1.3$ (Figure 2f). In particular, the vertical branch for $\kappa_{eff} = 2$ is centered near 28° initial pitch angle, which is larger than the pitch angle obtained for $\kappa_{eff} = 1.3$, of the order of 22°. This result is at odds with the single-hump case where the vertical branch occurs at larger and larger pitch angle as κ decreases toward unity (see Figure 1 of *Delcourt et al.* [1996a]). Also, it is apparent from Figure 2 that, for given κ_{eff} value, the computed pattern of μ variations significantly depends upon the magnitude of B_n (left and right panels). As an example, for $\kappa_{eff} = 2.0$, the vertical branch is centered near 24° pitch angle for $B_n = 0.5$ nT (Figure 2b) as opposed to 28° pitch angle for $B_n = 2.0$ nT (Figure 2e). A dependence of the μ_2/μ_0 patterns upon B_n can also be seen for $\kappa_{eff} = 1.3$ in the bottom panels of Figure 2. This result again contrasts with that obtained in the single-hump case where the envelope of μ variations does not change once κ is prescribed.

3. Centrifugal Impulse Model in a Double-Hump Geometry

[10] It was shown by *Delcourt et al.* [1994] that the nonadiabatic particle behavior at $\kappa \sim 1$ can be viewed as the result of an impulsive centrifugal force perturbing the

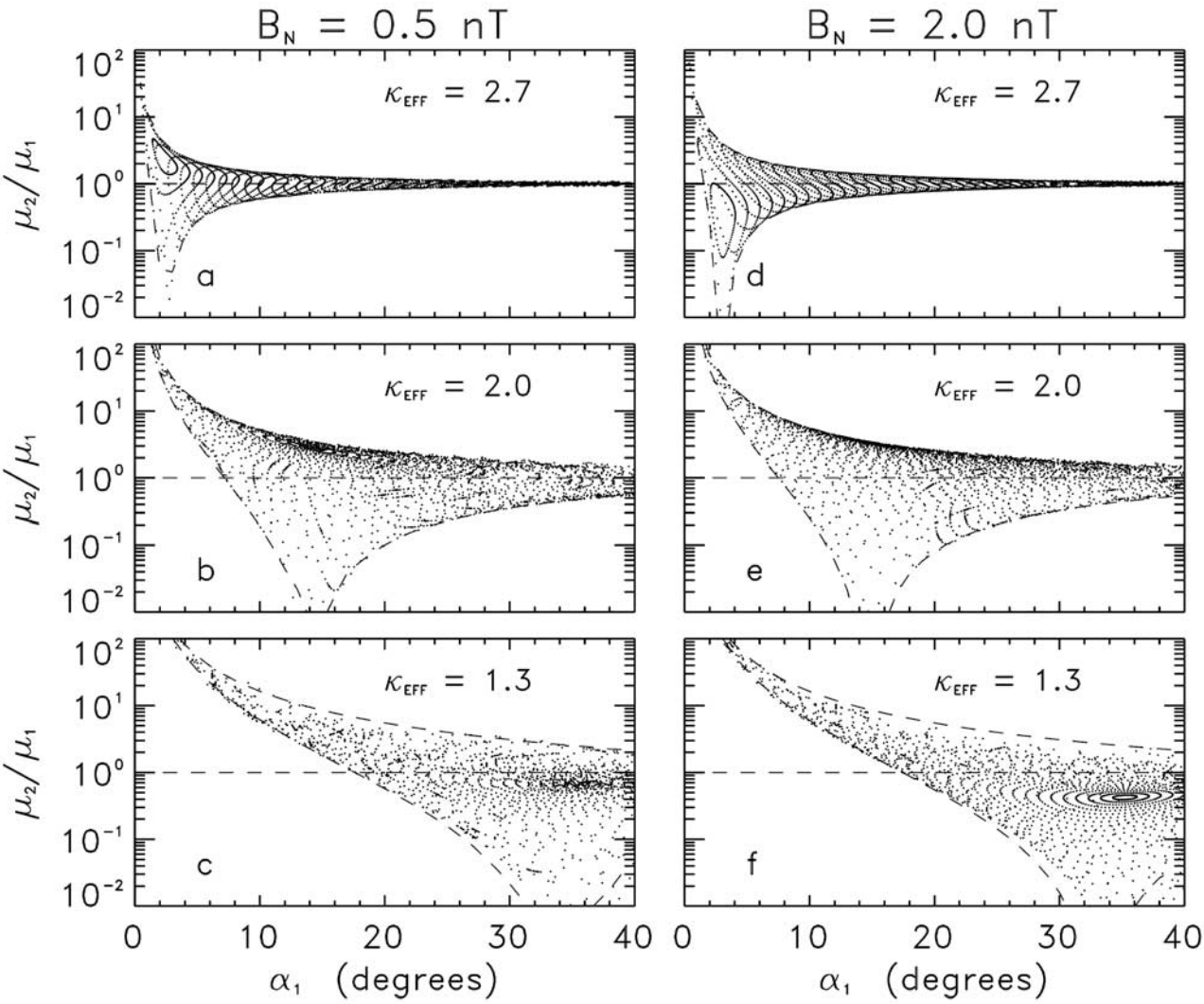

Figure 6. Identical to Figure 4 but for the final magnetic moment (normalized to that at $Z = 0$) as a function of pitch angle before crossing of the second hump. The dashed lines in each panel show the μ_1/μ_0 envelope achieved in Figure 4.

gyromotion during a critical cyclotron turn near the field minimum. *Delcourt and Martin* [1994] showed that this centrifugal impulse interpretation framework may be applied to the near-Earth magnetotail and leads to a three-branch pattern of μ variations that closely resembles that obtained from single particle trajectory computations, namely, systematic μ enhancements at small pitch angles, negligible μ change at large pitch angles, and in between either μ enhancement or damping depending upon phase. Also, *Delcourt et al.* [1996b] demonstrated that the oblique branch at small pitch angle goes together with prominent bunching in gyration phase, whereas a uniform phase spread is obtained for the horizontal (adiabatic) branch at large pitch angles (see, e.g., Figure 3 of *Delcourt et al.* [1996b]).

[11] Figure 3 shows an example of particle trajectories in the above double-hump configuration (equation (1)). As in Figure 1, B_o, B_n and L were set to 10 nT, 2 nT and 1 R_E, respectively. The particles were launched from $Z = L$, considering an initial pitch angle of 2° (at Z_K and using μ conservation) and distinct initial phases of gyration (from 0° to 360° by steps of 10°). Figure 3b indicates that after crossing of the field reversal, the test particles have a magnetic moment that is significantly larger (above 2 orders of magnitude) than the initial one, as evidenced from the large helical motion at $Z < 0$ in Figure 3a. In Figure 3e, bunching of the particles in gyration phase is also noticeable. Figure 3c which shows the centrifugal force experienced by the particles is of particular interest as it displays two successive enhancements centered near Z_K above and below the midplane (dotted lines). A comparison of Figures 3b, 3c, and 3e reveals that both magnetic moment and gyro-phase changes are closely correlated with these enhancements. In contrast, no magnetic moment change is observed near $Z = 0$ where B is minimum and the magnetic field line curvature negligible. In other words, nonadiabatic episodes occur where the field line curvature maximizes and this leads us to examine the particle behavior in Figure 3 in terms of repeated application of the centrifugal impulse model (CIM) described above.

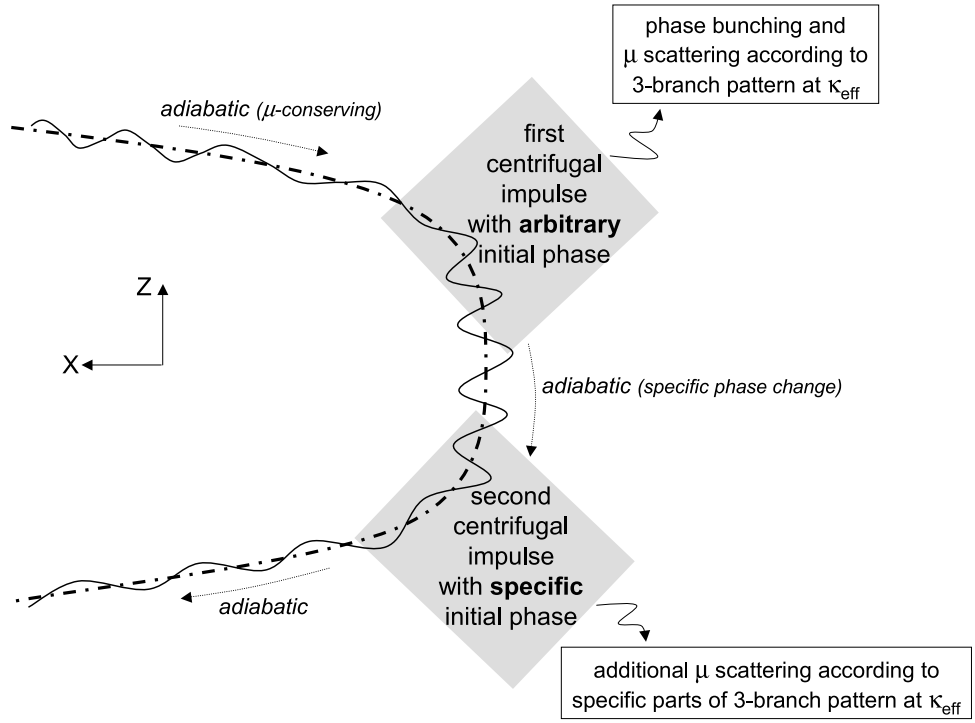

Figure 7. Schematic illustration of the successive centrifugal impulses acting upon the particles during interaction with a double-hump current sheet.

[12] It was shown in Figure 2 that the net change of magnetic moment after interaction with a double-hump current sheet differs from that obtained in a single-hump one. On the other hand, Figure 3 reveals that μ changes in the double-hump case do occur in conjunction with centrifugal impulses, in a very like manner to the single-hump case. Figure 3 however exhibits two successive centrifugal impulses and we anticipate that if we consider only one of these, the CIM interpretation framework will hold. We accordingly placed ourselves at $Z = 0$ (i.e., immediately after the first centrifugal impulse in Figure 3) and recorded the local magnetic moment of the particles. The results of these calculations are shown in Figure 4 using a format similar to that of Figure 2. Several features of interest are noticeable in Figure 4. First, it can be seen that regardless of B_n and κ_{eff}, clear three-branch patterns of μ variations are obtained. For given B_n, these patterns gradually evolve toward larger and larger pitch angles as κ_{eff} decreases

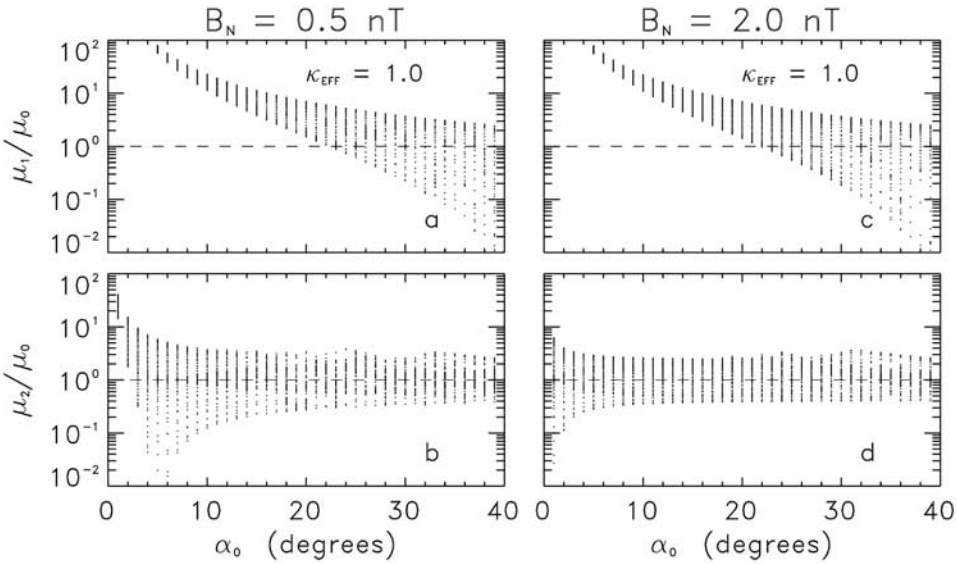

Figure 8. Magnetic moment as a function of initial pitch angle for $\kappa_{eff} = 1.0$: (top) at $Z = 0$ and (bottom) after the second hump. Left and right panels correspond to two different values of B_n (namely, 0.5 and 2.0 nT, respectively).

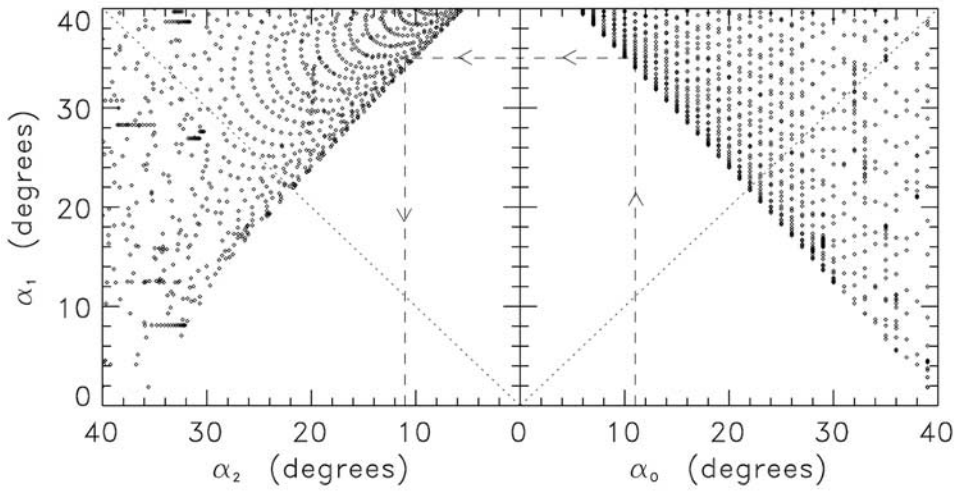

Figure 9. (right) Pitch angle after the first hump as a function of initial pitch angle and (left) final pitch angle (in abscissa) as a function of pitch angle after the first hump for the case $\kappa_{eff} = 1.0$ and $B_n = 2.0$ nT (right panels of Figure 8). The various dots correspond to different initial pitch and phase angles.

toward unity. Also, for given κ_{eff}, a specific three-branch pattern is obtained that does not depend upon the magnitude of B_n, quite consistent with the definition of κ. These results are in agreement with the CIM interpretation framework (see, e.g., Figure 1 of *Delcourt et al.* [1996a]) and contrast with those achieved in Figure 2.

[13] Figure 4 thus demonstrates that the centrifugal impulse model is appropriate to characterize the particle interaction with the first hump. We then expect this model to be valid as well upon interaction with the second hump. At this stage however, particles have already been subjected to three-branch scattering and we expect that they will not experience the second centrifugal impulse in an arbitrary manner. To illustrate this, Figure 5 shows the effect of repeated application of the analytical three-branch pattern at $\kappa = 1.3$ (equations (1)–(2) of *Delcourt et al.* [1996b]), assuming distinct phase changes between the two successive centrifugal impulses (namely, 60° and 160° in the left and right panels, respectively). If we consider an initial pitch angle of 4° and different initial phases of gyration (from 0° to 360° by steps of 20°), it can be seen in Figure 5 that the first impulse yields a large (up to about two orders of magnitude; closed circles labelled 1) magnetic moment enhancement regardless of initial gyration phase. As a result, particles exhibit pitch angles between ~30° and ~40° prior to the second impulse. If we then assume an overall phase change of 60° between the two impulses (left panel), it can be seen that the particles experience μ enhancement by about a factor 2, whereas an overall phase change of 160° (right panel) leads to μ damping by about one order of magnitude (closed circles labelled 2).

[14] Although the basic pattern of μ variations has a simple three-branch structure, Figure 5 thus suggests that repeated application of this pattern may lead to complex μ changes. Still, if the CIM interpretation framework is valid, magnetic moments after the second hump normalized to those obtained after the first hump should exhibit three-branch patterns similar to those in Figure 4. Figure 6 which shows the μ_2/μ_1 ratio as a function of α_1 confirms this outcome. The patterns portrayed in this figure closely resemble those in Figure 4, namely, for given κ_{eff} value, all μ variations are confined within the same envelope (dashed lines) regardless of B_n. Also, for given B_n, the μ variations gradually extend toward larger and larger pitch angles as κ_{eff} decreases (see, e.g., Figures 6d, 6e, and 6f). Moreover, as expected from Figure 5, it is apparent that the various regions of the three-branch patterns are not covered in a uniform manner and locally exhibit fine structuring due to specific phase gains.

4. Discussion

[15] Figure 7 schematically summarizes the interpretation framework developed above. In contrast to a single-hump field reversal where the nonadiabatic behavior at $\kappa \approx 1$ may be reduced to a critical cyclotron turn near $Z = 0$, the particle behavior in a double-hump geometry can be viewed as the result of two successive centrifugal impulses on either side of the midplane. After adiabatic (μ-conserving) approach of the field reversal, a first impulse occurs near the locus of maximum curvature off-equator, which leads to μ scattering according to three branches as in the single-hump case. During this interaction, bunching in gyration phase occurs for particles with relatively small pitch angles. Subsequently, after crossing of the $Z = 0$ plane, particles are subjected to a second impulse at a distance from the equator that is comparable to that of the previous one. This latter impulse yields a pattern of μ variations virtually identical to the previous one, this pattern being solely determined by the value of κ_{eff}. However, the succession of the two impulses is such that phase coherence is maintained and interaction with the second hump does not fill the three branches in a uniform manner. In other words, the complex magnetic moment variations achieved in a double-hump current sheet may be decomposed in elemental scattering sequences that can each be described with the help of the centrifugal impulse model. Though out of the scope of the present

study, we may speculate that such a description will be valid as well for current sheet structures that exhibit more than two humps.

[16] The comparison of Figures 2e and 2f indicates that the net μ change experienced by the particles may weaken as κ_{eff} decreases toward unity, a situation which contrasts with that prevailing in a single-hump configuration. To provide further insights into this effect, Figure 8 presents the results of numerical trajectory calculations for $\kappa = 1.0$. As in Figure 2, two distinct values of B_n were considered (namely, 0.5 nT and 2 nT in the left and right panels, respectively). The top panels of Figure 8, which show the μ variations obtained after the first hump, display an oblique branch that extends over a large (up to $\sim 30°$) pitch angle interval. This branch does not depend upon the magnitude of B_n, being solely controlled by the value of κ_{eff}. This result differs from the patterns achieved in the bottom panels of Figure 8 which show the μ variations obtained after the second hump. For $B_n = 0.5$ nT (Figure 8b), a three-branch pattern can be seen that features magnetic moment damping for initial pitch angles of $\sim 6°$. In contrast, for $B_n = 2$ nT (Figure 8d), the three-branch structuring nearly vanishes, the μ_2/μ_o ratio being of the order of unity throughout most of the pitch angle range considered. In *Büchner and Zelenyi* [1989], particles that execute Speiser-type orbits at $\kappa < 1$ were referred to as quasi-adiabatic. Indeed, though these particles meander inside the neutral sheet and do not behave adiabatically stricto senso, they escape from the field reversal with a magnetic moment nearly identical to that at entry. Such quasi-adiabatic behaviors clearly resemble those displayed in Figure 8, though they relate to a different κ range than that considered in the present study ($\kappa \approx 1$).

[17] The quasi-adiabatic behavior portrayed in Figure 8d can be better appreciated in Figure 9 which shows the successive particle pitch angles (evaluated at Z_K using μ conservation) during interaction with the two humps. Each dot in this figure corresponds to given initial pitch and phase angles. The right panel of Figure 9 shows the pitch angles after crossing of the first hump as a function of initial pitch angles. As expected from three-branch μ variations, it is apparent from this panel that particles with small initial pitch angles subsequently have much larger pitch angles whereas those with large initial pitch angles subsequently have either small or large pitch angles depending upon gyration phase. The left panel of Figure 9 shows the pitch angles after the second hump (i.e., at exit from the field reversal) versus those after the first hump. It is apparent from this latter panel that particles with large intermediate pitch angles α_1 may exhibit small final pitch angles α_2 and vice versa. In fact, turning the left panel of Figure 9 by 90° in the clockwise direction, one obtains a pattern which resembles that in the right panel, though some additional structuring is noticeable due to phase bunching upon interaction with the first hump. As an example, consider a particle with $\alpha_0 = 11°$ (dashed line in the right panel of Figure 9). For this particle, interaction with the first hump leads to μ enhancement and $\alpha_1 \approx 35°$, whereas the subsequent interaction with the second hump leads to μ damping and $\alpha_2 \approx \alpha_0$. Though it occurs in a different κ range and field geometry, such a behavior indeed is reminiscent of the I_Z jumps put forward by *Büchner and Zelenyi* [1989] to characterize quasi-adiabatic (Speiser-type) orbits.

5. Conclusion

[18] The simulations performed demonstrate that the double-hump current sheets that develop during the late growth phase of substorms lead to a wide variety of nonadiabatic particle behaviors. These behaviors may be viewed as successions of elemental scattering sequences that can each be described using the centrifugal impulse model developed for single-hump current sheets. That is, the net magnetic moment change experienced by the particles follows from perturbation of their gyro-motion by successive centrifugal impulses that do not occur at the equator but at some distance from it where the magnetic field line curvature maximizes. Each of these impulses leads to a three-branch pattern of magnetic moment variations as in the single-hump case. The characteristics of this three-branch pattern are solely controlled by the parameter κ_{eff} which resembles the usual adiabaticity parameter κ but which is evaluated off-equator. For given κ_{eff}, gyrophase gains during the first impulse as well as between the impulses are found to play a critical role in the net magnetic moment variations, possibly leading to quasi-adiabatic behavior with negligible μ change at $\kappa_{eff} = 1$.

[19] **Acknowledgments.** We thank F. V. Coroniti and V. A. Sergeev for stimulating discussions. This work was supported by Russian Foundation of Basic Research grants 02-02-16003, 02-05-64184 and Scientific Schools grant HIII-1739.2003.2.

[20] Arthur Richmond thanks Donald Mitchell and Victor Sergeev for their assistance in evaluating this paper.

References

Asano, Y., T. Mukai, M. Hoshino, Y. Saito, H. Hayakawa, and T. Nagai (2003), Evolution of the thin current sheet in a substorm observed by Geotail, *J. Geophys. Res.*, *108*(A5), 1189, doi:10.1019/2002JA009785.

Büchner, J., and L. M. Zelenyi (1989), Regular and chaotic charged particle motion in magnetotaillike field reversals: 1. Basic theory of trapped motion, *J. Geophys. Res.*, *94*, 11,821.

Burkhart, G. R., and J. Chen (1991), Differential memory in the Earth's magnetotail, *J. Geophys. Res.*, *96*, 14,033.

Chen, J., and P. J. Palmadesso (1986), Chaos and nonlinear dynamics of single-particle orbits in magnetotaillike magnetic field, *J. Geophys. Res.*, *91*, 1499.

Chen, J., H. G. Mitchell, and P. J. Palmadesso (1990a), Differential memory in the trilinear model magnetotail, *J. Geophys. Res.*, *95*, 15,141.

Chen, J., G. R. Burkhart, and C. Y. Huang (1990b), Observational signatures of nonlinear magnetotail particle dynamics, *Geophys. Res. Lett.*, *17*, 2237.

Delcourt, D. C., and R. F. Martin Jr. (1994), Application of the centrifugal impulse model to particle motion in the near-Earth magnetotail, *J. Geophys. Res.*, *99*, 23,583.

Delcourt, D. C., R. F. Martin Jr., and F. Alem (1994), A simple model of magnetic moment scattering in a field reversal, *Geophys. Res. Lett.*, *21*, 1543.

Delcourt, D. C., J.-A. Sauvaud, R. F. Martin Jr., and T. E. Moore (1996a), On the nonadiabatic precipitation of ions from the near-Earth plasma sheet, *J. Geophys. Res.*, *101*, 17,409.

Delcourt, D. C., G. Belmont, J.-A. Sauvaud, T. E. Moore, and R. F. Martin Jr. (1996b), Centrifugally driven phase bunching and related current sheet structure in the near-Earth magnetotail, *J. Geophys. Res.*, *101*, 19,839.

Galeev, A. A., and L. M. Zelenyi (1975), Metastable states in the diffusion neutral layer and explosive phase of substorm, *JETP Lett.*, *12*, 170.

Greco, A., A. L. Taktakishvili, G. Zimbardo, P. Veltri, and L. M. Zelenyi (2002), Ion dynamics in the near-Earth magnetotail: Magnetic turbulence versus normal component of the average magnetic field, *J. Geophys. Res.*, *107*(A10), 1267, doi:10.1029/2002JA009270.

Harris, E. G. (1962), On a plasma sheath separating regions of oppositely directed magnetic fields, *Nuovo Chimento*, *23*, 115.

Holland, D. L., W. R. Paterson, L. A. Frank, S. Kokubun, and Y. Yamamoto (1999), Signatures of nonlinear charged particle dynamics in Geotail Comprehensive Plasma Instrument observations, *J. Geophys. Res.*, *104*, 2479.

Hoshino, M., A. Nishida, T. Mukai, Y. Saito, and T. Yamamoto (1996), Structure of plasma sheet in magnetotail: Double-peaked electric current sheet, *J. Geophys. Res.*, *101*, 24,775.

Mitchell, D. G., D. J. Williams, C. Y. Huang, L. A. Frank, and C. T. Russell (1990), Current carriers in the near-Earth cross-tail current sheet during substorm growth phase, *Geophys. Res. Lett.*, *17*, 583.

Nakamura, R., et. al (2002), Fast flow during current sheet thinning, *Geophys. Res. Lett.*, *29*(23), 2140, doi:10.1029/2002GL016200.

Pulkkinen, T. I., D. N. Baker, D. G. Mitchell, R. L. McPherron, C. Y. Huang, and L. A. Frank (1994), Thin current sheets in the magnetotail during substorms: CDAW 6 revisited, *J. Geophys. Res.*, *99*, 5793.

Runov, A., et al. (2003a), Current sheet structure near magnetic X-line observed by Cluster, *Geophys. Res. Lett.*, *30*(A11), 1579, doi:10.1029/2002GL016730.

Runov, A., R. Nakamura, W. Baumjohann, T. I. Zhang, and M. Volverk (2003b), Cluster observation of a bifurcated current sheet, *Geophys. Res. Lett.*, *30*(2), 1036, doi:10.1029/2002GL016136.

Sergeev, V. A., D. G. Mitchell, C. T. Russell, and D. J. Williams (1993a), Structure of the tail plasma/current sheet at 11 Re and its changes in the course of a substorm, *J. Geophys. Res.*, *98*, 17,345.

Sergeev, V. A., M. Malokov, and K. Mursula (1993b), Testing the isotropic boundary algorithm method to evaluate the magnetic field configuration in the tail, *J. Geophys. Res.*, *98*, 7609.

Sergeev, V. A., V. Angelopoulos, C. Carlson, and P. Sutcliffe (1998), Current sheet measurements within a flapping plasma sheet, *J. Geophys. Res.*, *103*, 9177.

Sergeev, V. A., et al. (2003), Current sheet flapping motion and structure observed by Cluster, *Geophys. Res. Lett.*, *30*(6), 1327, doi:10.1029/2002GL016500.

Speiser, T. W. (1965), Particle trajectory in model current sheets: 1. Analytical solutions, *J. Geophys. Res.*, *70*, 4219.

Zelenyi, L. M., D. C. Delcourt, H. V. Malova, and A. S. Sharma (2002), ''Aging'' of the magnetotail thin current sheets, *Geophys. Res. Lett.*, *29*(12), 1608, doi:10.1029/2001GL013789.

D. C. Delcourt, CETP-CNRS-IPSL, 4 Avenue de Neptune, 94107 Saint-Maur des Fosses, France. (dominique.delcourt@cetp.ipsl.fr)

H. V. Malova, Nuclear Physics Institute, Moscow State University, Leninskie Gory, 119992 Moscow, Russia. (mlv@dec1.sinp.msu.ru)

L. M. Zelenyi, Space Research Institute, Russian Academy of Sciences, Profsoyuznaya Street 84/32, GSP-7, 117997 Moscow, Russia. (lzelenyi@iki.rssi.ru)